Final Draft
of the original manuscript:

Zerbst, U.; Schoedel, M.; Heyder, R.:
Damage tolerance investigations on rails
In: Engineering Fracture Mechanics (2008) Elsevier

DOI: 10.1016/j.engfracmech.2008.04.001

DAMAGE TOLERANCE INVESTIGATIONS ON RAILS

Uwe Zerbst [a], Manfred Schödel [b] & Rene Heyder [c]

[a] GKSS Research Centre, Institute for Materials Research, Materials Mechanics, D-21502 Geesthacht, Germany

[b] former GKSS Research Centre, now ALSTOM, CH-5401 Baden, Swizerland

[c] Deutsche Bahn AG, DB Systemtechnik (TZF 93), D-14774 Brandenburg-Kirchmöser, Germany

Abstract: The paper summarises damage tolerance investigations on railway rails which the authors have carried out in the context of the German-French joint project NOVUM (Novel methods for quantitative prediction of rail performance at increased service loads) [1]. The investigations include the determination of the crack driving force as a function of the various loading components a rail is subjected to and the simulation of residual lifetime. Features such as the local load input at the rail-wheel interface, dynamic effects and statistical aspects of crack resistance are explicitly taken into account.

Keywords: Railway rails, transverse cracks, damage tolerance, fatigue crack propagation, residual lifetime.

1. INTRODUCTION

The avoidance of rail failure is a primary goal of track safety. Although, in reality, not many broken rails cause derailment there are a few cases of extremely severe consequences. An example was the Hatfield accident in October 2000 where four people died and a further 70 were injured [2]. As has been shown for Britain [3], whilst failures of railway wheels and axles have been reduced by a factor of 20 over the last hundred years, the number of rail failures per train kilometre has even increased. The main reasons are heavier axle loads and thermal stresses at low ambient temperatures in continuously welded tracks. Although a lot of effort has been spent on the problem of rail failure over the last decades ([4] see also [5,6]) it remains a rather difficult one. This paper addresses one aspect of the failure scenario: the final stage of fatigue crack extension and its termination by brittle fracture.

2. LOADING AND FATIGE CRACK PROPAGATION – GENERAL ASPECTS

Railway rails are subjected to highly complex loading conditions (Fig. 1, for a more detailed discussion see [4]). The various loading components are:

(a) Thermal stresses

Thermal stresses occur in continuously welded rails at ambient temperatures different to the temperature at track installation - the “rail neutral temperature”. At higher ambient temperatures at hot summer days the rail is compression loaded. Because it is prevented from thermally expanding in the axial direction there is the danger of lateral buckling which, if large enough, may cause derailment. In contrast, at temperatures lower than the neutral temperature tensile thermal stresses are built up which reach their maximum at cold winter nights.

(b) Residual stresses

Residual stresses are introduced by heat treatment and roller straightening during the manufacturing process. The residual stress field is characterised by axial tensile stresses in the head and foot of the rail counterbalanced by compression in the web. Since the residual stress state at, and some millimetres below, the running surface will be modified in service due to the wheel-rail contact the peak residual tensile stress is shifted to the centre of the rail head whereas the contact area is subjected to compressive residual stresses. Another source of residual stresses is butt welding which, however, shows a different pattern.

(c) Stresses due to axle loading

Typical axle loads are in the range of 21 to 25 tons but can be up to 37 tons for example in iron-ore trains [5]. Axle loads generate bending and shear stresses in the rail which might be significantly increased by dynamic effects. Note that the magnification is strongly affected by shape irregularities of the rails as well as of the wheels but also by variations in the track foundation. Besides the dominating vertical bending loading, lateral bending also occurs.

(d) Wheel-rail contact stresses

Because the contact stresses are extremely high, they almost exclusively control the early damage process at the running surface including crack nucleation and early crack growth (rolling contact fatigue). These stresses are caused by the dynamic axle loads but also by forces in the wheel-rail contact area due to traction, braking or steering. Contact stresses decline rapidly in the depth direction.

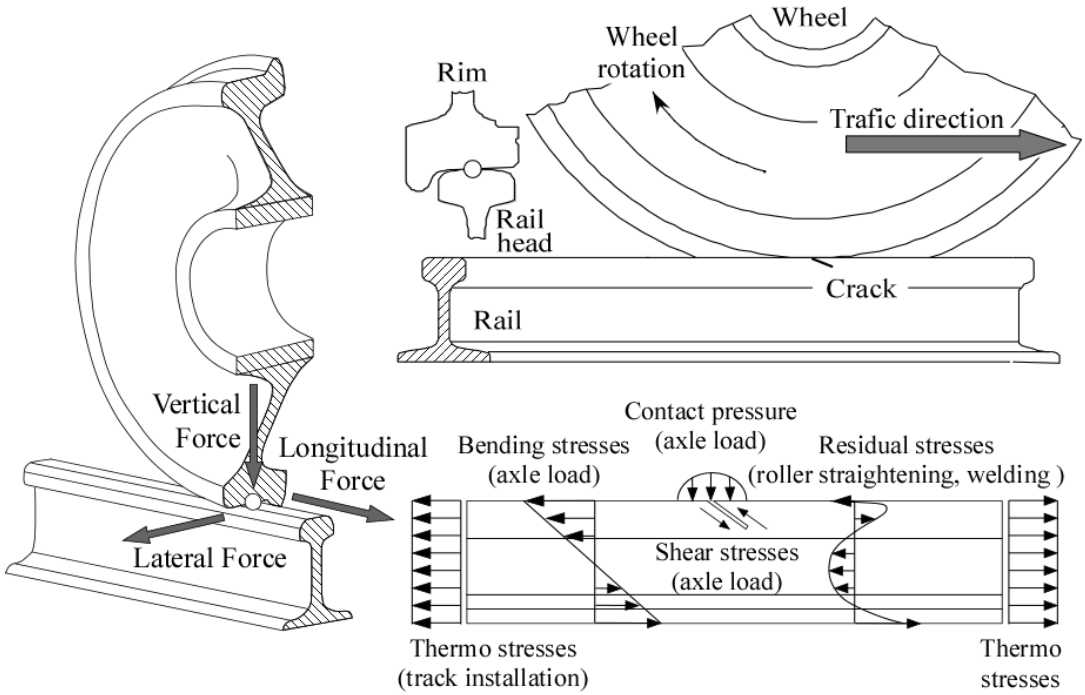

Figure 1: Loading configuration of a rail.

This complex loading state has far-reaching consequences for the nucleation and propagation of potential fatigue cracks. Two of them are addressed in the following:

(a) As outlined in [4], once a fatigue crack has been nucleated its extension can roughly be subdivided into two stages (Figure 2). At Stage 1 the crack grows at a shallow angle of 10 to 40^{o} to the running surface. Its propagation is predominantly controlled by the contact stress field. After it has reached a certain length and - in conjunction with this - a certain depth usually larger then 5 mm [7] the crack changes its propagation direction either upwards to the running surface or downwards to the web. In the first case the consequence is surface spalling, in the second it is transverse crack growth up to rail breakage. The Stage 2 crack propagation angle with respect to the running surface is 60 to 80^{o} or more for tracks operated in one direction. It is controlled by the bulk stresses.

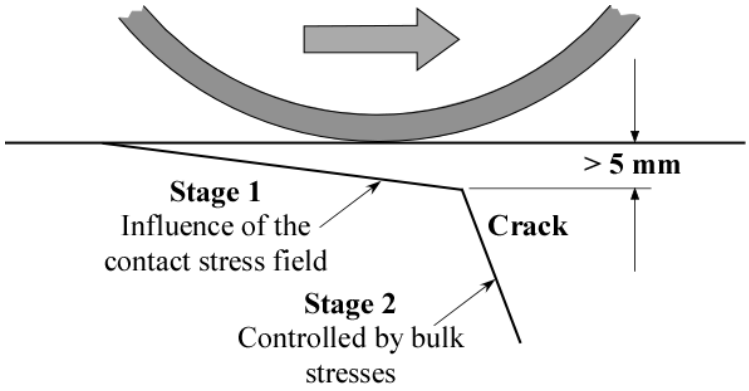

Figure 2: Two stages of fatigue crack propagation.

(b) Rail cracks are out-of-phase mixed mode loaded with mode II being the dominant component such as illustrated for a point at the front of an angular semi-elliptical surface crack in Figure 3 [8]. When the vehicle wheel approaches the crack site the point under consideration is loaded by a moderate mode I cycle due to rail bending. It then follows a much higher mode II cycle and - only slightly out-of-phase to this - a mode III cycle when the wheel passes over the crack. Note that the crack propagation rate as well as the size at which the crack deviates from the Stage 1 to the Stage 2 plane is influenced by the presence of lubricant, usually water. [9].

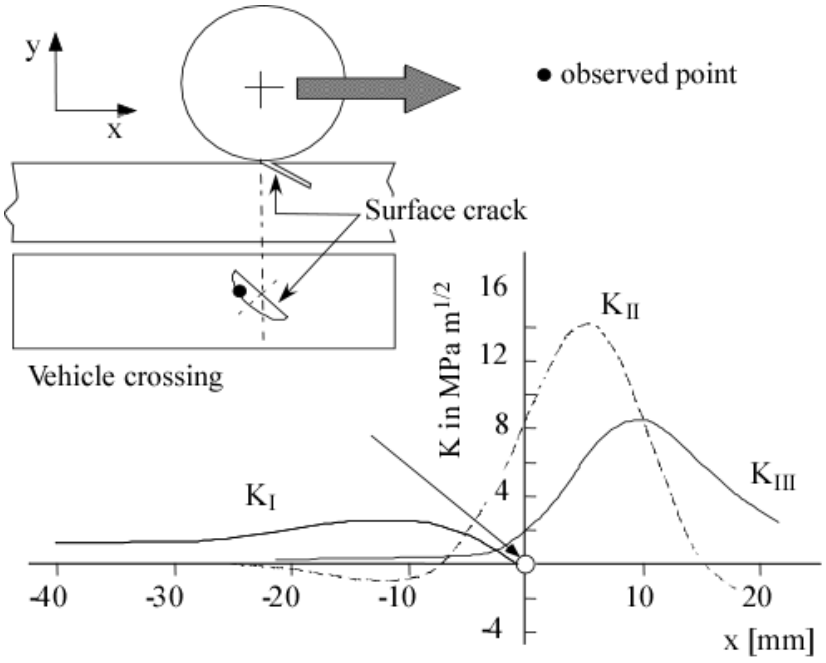

Figure 3: Mixed mode loading sequence of a surface crack during wheel pass over (according to [8]).

3. DAMAGE TOLERANCE INVESTIGATIONS

3.1 Assumptions for Fatigue Crack Propagation

The present study concentrates on Stage 2 crack propagation, i.e., the crack propagation after the crack deviated in transverse direction. It is well known that this stage is much shorter in time than Stage 1. However, in contrast to real conditions, an initial depth of only 1 or 2 mm was assumed for the Stage 2 crack (Figure 4) in the following. The idea behind this assumption is that it would allow a conservative estimate of the complete (Stages 1 + 2) crack propagation. The likelihood of detection of such small initial crack sizes during non-destructive inspection is realistic when eddy current techniques are applied rather than ultrasonics [10]. Note that the initial crack size assumed in a damage tolerance analysis has to be equal or larger than the detection limit of the applied inspection method under service conditions.

The rail head was assumed to be uniformly worn by 10 mm such as shown in Figure 5.

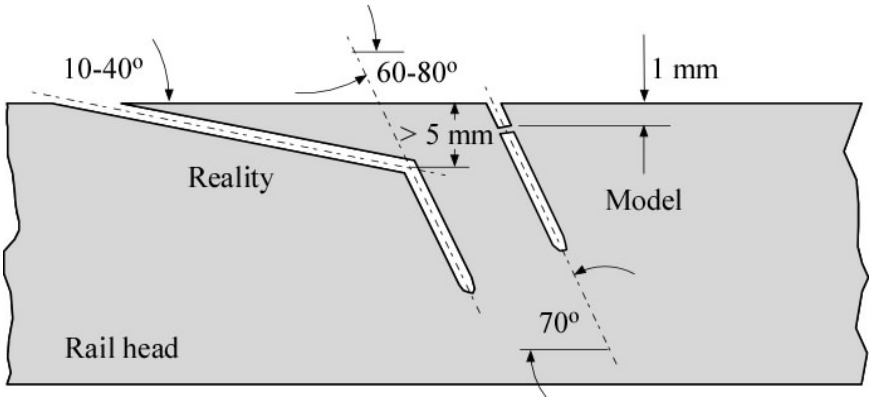

Figure 4: Crack configuration of the present model. Basic assumption.

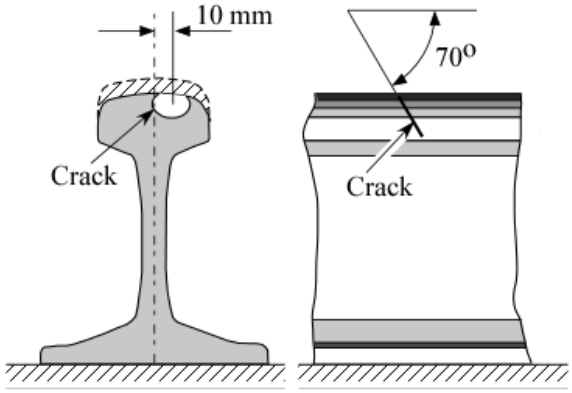

Figure 5: Crack configuration of the present model: Left: The worn rail head; Right: The assumed transverse fatigue crack extension path.

3.2 Loading

The loading of the rail due to the train was simulated as a multi-body system including vehicle and track and was calibrated by in-field measured data. In addition to the vertical and lateral forces also the vertical displacements of the sleepers were determined. The vertical load including its time-dependent dynamic magnification during the pass-over of a high-speed train is illustrated in Figure 6.

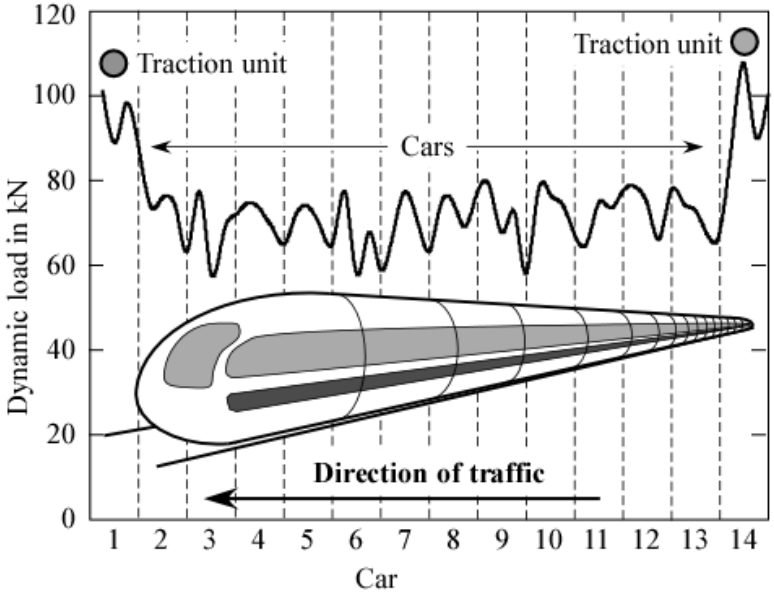

Figure 6: Vertical load at the rail during the pass-over of a high-speed train (data provided by Deutsche Bahn (DB) Systemtechnik, TZF 62).

3.3 Crack Driving Force

Stress intensity factors were determined by finite element analyses for the fifteen crack configurations shown in Figure 7. For each of these cracks K_I, K_{II} and K_{III} factor solutions were provided for the deepest (A) and the most extended horizontal points (B,C), for thermal and residual stresses and for axle loading. The results are summarised as tables in the Appendix. Neutron scatter residual stress profiles were provided by Corus Rail, Hayange [11]. The axial residual stress component is shown in Figure 8. Since the measurements were based on horizontal and vertical slices of 10 mm thickness and covered only the rail head area and the vertical centre line from head to foot preliminary processing of the field data was necessary before their use in the analyses. The available data were added by measuring points of another rail at further positions [12]. Finally the data were slightly modified such that the resulting residual stress field was adjusted to make it self-equilibriating after the first iteration step, in order not to cause the bending of the rail. However, the axial residual stress component was kept almost identical to the originally measured data. Note that the resulting residual stress field, therefore, is an estimate but, in the authors' opinion not far from reality. In the future finite element process simulations (see e.g. [13]) should provide enhanced information.

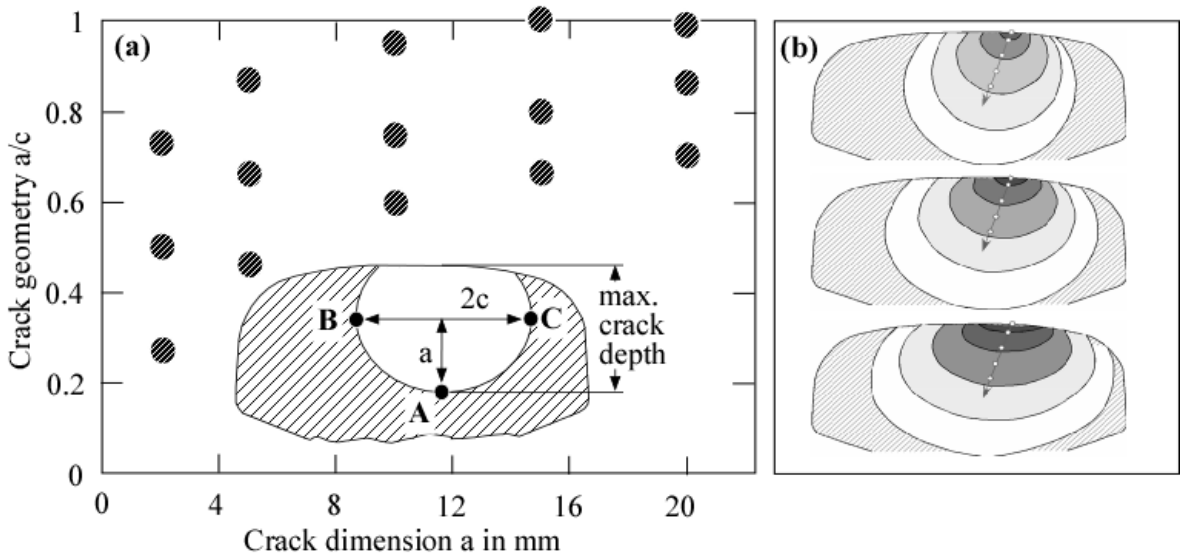

Figure 7: All crack configurations for which K factor solutions were determined by finite element analyses.

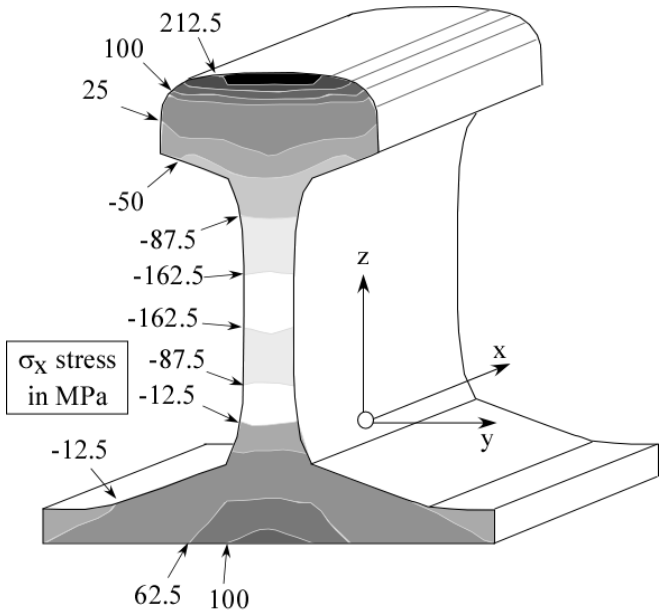

Figure 8: Processed residual stress profile. Only the axial stress component is shown.

The specification of K factor solutions for axle loading was faced with a two major problems:

(a) Due to the dynamic effects during pass-over no unique correlation exists between the vertical loads and the K factor components. In order to avoid the effort of a fully dynamic analysis the determination of the K factors was based on the vertical loads and the corresponding average vertical displacement of the sleeper such as shown in Figure 9.

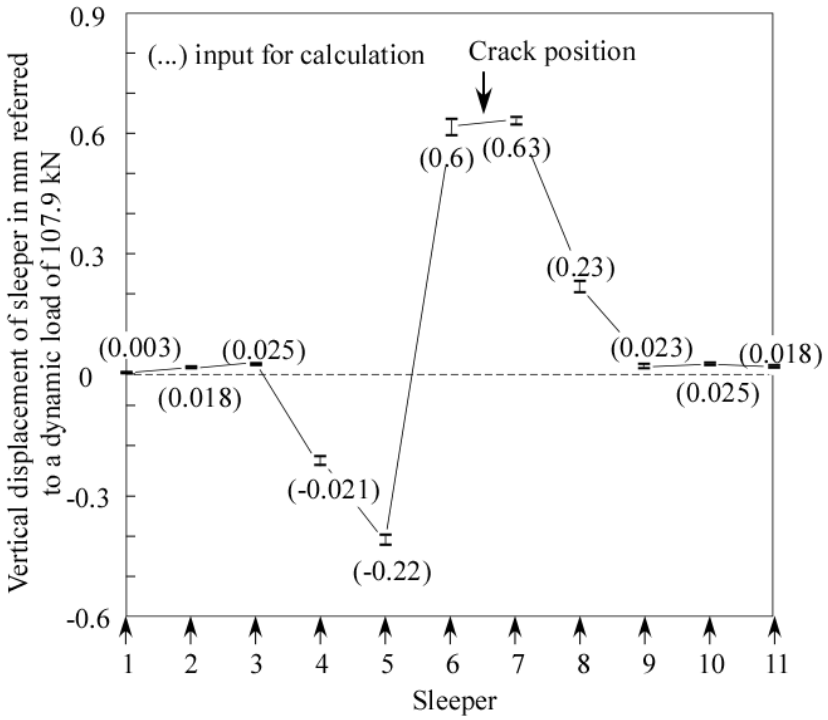

Figure 9: Vertical displacement of the sleepers corresponding to a dynamic load of 107.9 kN (dynamic axle load of a traction unit) during a pass-over of a high-speed train.

(b) The second problem is caused by the fact that the local load input occurs next to the crack position. Therefore, varying cross-over paths from wheel to wheel, e.g. due the common side motion of the bogie, is expected to be significant for the crack driving force at different positions of the crack front. In order to model this, K factor solutions were obtained for four different roll-over paths (Figure 10) which where than statistically mixed in the final fatigue crack growth analyses. For a realistic simulation the contact between wheel and rail was modelled using a simplified wheel geometry instead of a point load (Figure 11).

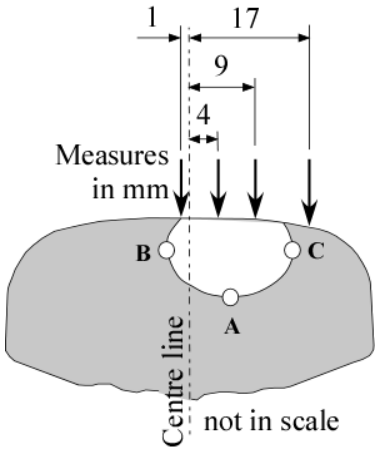

Figure 10: Roll-over paths for which sets of K factor solutions were determined (see the Appendix).

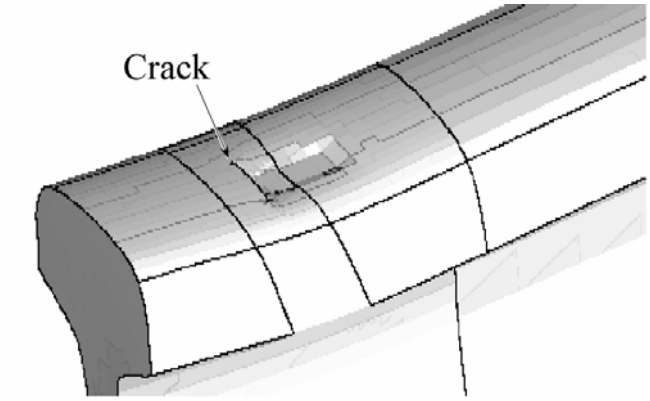

Figure 11: Example of a finite element simulated indentation of the wheel into the rail in the context of the K factor determination for axle loading.

Any fatigue crack extension analysis requires the determination of equivalent mixed mode stress intensity factor solutions K_v for the various loading components. The equivalent K factor range ΔK_v can easily be obtained by

$$\Delta K_v = \frac{\Delta K_I}{2} + \frac{1}{2}\sqrt{\Delta K_I^2 + 4\,\left(1.155\,\Delta K_{II}\right)^2 + 4\,\Delta K_{III}^2} \qquad (1)$$

[14] for proportional loading, i.e., the loading components occur simultaneously. However, this assumption is wrong as already shown in Figure 3 where the loading components are out-of-phase. That means that the maximum and minimum K factors K_{max} and K_{min} due to the individual loading components will occur at different times or vehicle positions with respect to the crack site. Therefore, in order to identify K_{max} and K_{min}, additional sets of finite element analyses referring to different wheel positions had to be carried out such as illustrated in Figure 12. Note that the mode-I-K factors were corrected for crack closure using the NASGRO approach [15].

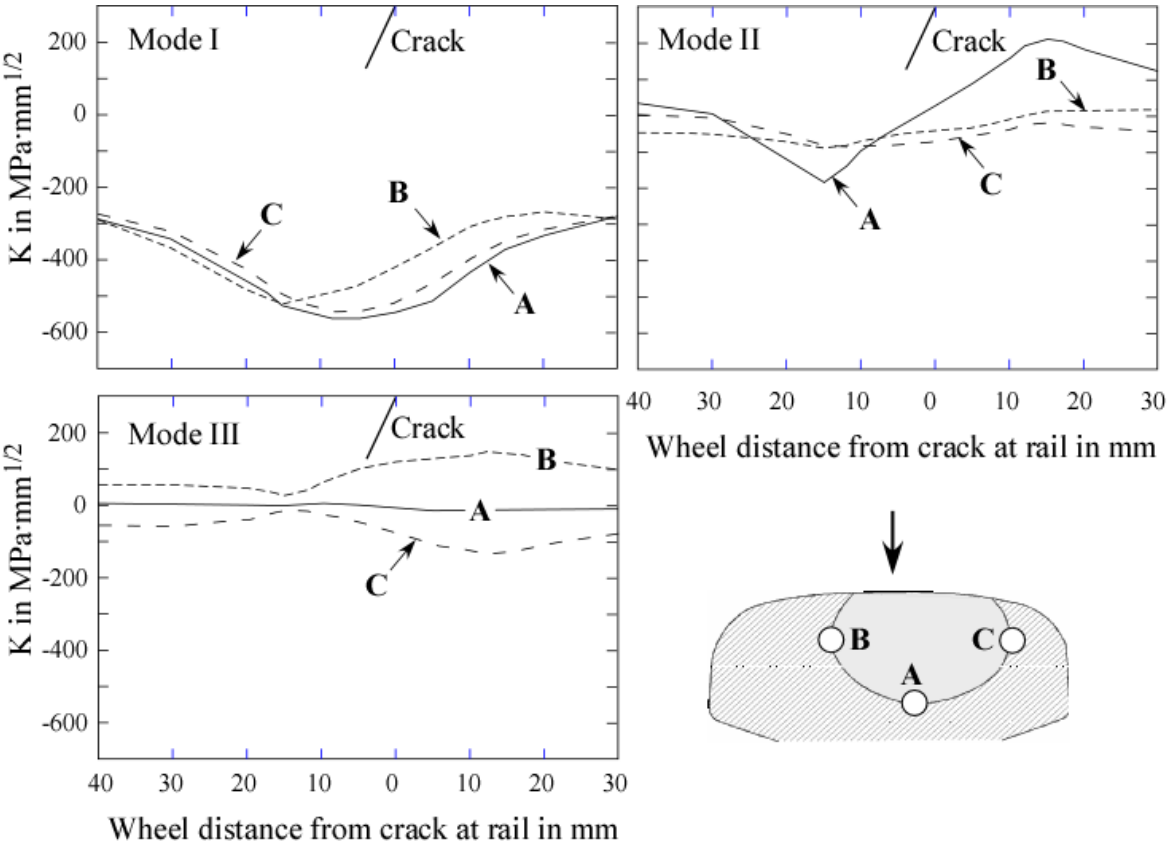

Figure 12: Example for the determination of K_{max} and K_{min} values for mode I, II and III as a function of the distance of the wheel contact area from the crack site.

3.4 Material Data

The information on the material needed for a damage tolerance analysis of a rail comprises fracture toughness and fatigue crack extension characteristics. In cases where significant ligament yielding is expected also the deformation behaviour of the material has to be available. This was, however, not necessary for the present analyses.

The fracture toughness data were determined for two temperatures and for vertical and horizontal crack orientations with respect to the rail head. The material, a R260 (former 900A) rail steel, showed pronounced pop-in behaviour because of which the toughness had to be defined by the first pop-in event in each test. The scatter in toughness was taken into account by statistical processing based on the VTT-Master Curve concept [16] (Figure 13). For more detailed information on this issue see [17]. With respect to fatigue crack extension out-of-phase mixed mode loading is expected to play a significant role. Therefore, the present analyses used an experimental mode I/mode II da/dN-ΔK_v curve of a rail steel provided in [18] as a first estimate:

$$da/dN = 5.86 \cdot 10^{-9} \Delta K_v^{3.12} \qquad (2)$$

with da/dN in mm/cycle and ΔK_v in MPa $m^{1/2}$ (load ratio $R = K_{min}/K_{max} = 0.5$).

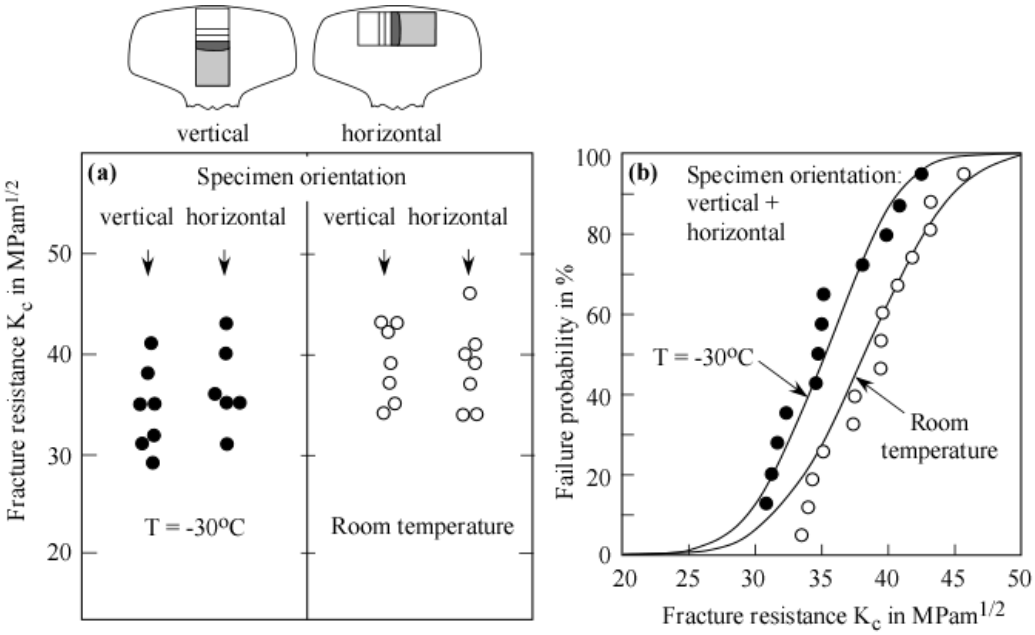

Figure 13: Scatter of fracture toughness for vertical and horizontal crack location in the rail head (a) and its statistical processing using the Master Curve concept (b). The data refer to 1T specimens, i.e., a crack front length of c. 25 mm.

3.5 The Effect of the Local Load Input

In order to examine the effect of the bogie's side motion on the fatigue crack extension dependent on the state of wear of both the rail and the wheels four rail-wheel combinations (rail and wheel new, rail and wheel worn, alternating only rail or wheel worn) were investigated (Figure 14). These where modelled by mixing the four roll-over paths for which K factors had been generated on a statistical basis such as summarised in Table 1. Note that the maximum frequency of roll-over events does not occur at the centre of the rail head but at a distance of 5 to 10 mm towards the inner side in new rails (Figure 14 b and d). Since any rail starts as a new one crack nucleation is to be expected at this site and that is what happens in a real track and has been modelled in the present paper (cf. Figure 5). When the rail, after a certain time in service, is worn the roll-over pattern changes (Figure 14 a and c) shifting the maximum frequency of roll-over events to the centre line of the rail head.

That this effect is significant for the damage tolerance behaviour of rails is illustrated by the results of Figure 15. As can be seen the rail-wheel combinations (2) and (4) (new rails) tend to the shortest residual lifetimes. The differences to combinations (1) and (3) are predominantly due to the early crack extension whilst the growth of the larger crack is of minor effect. Note, however, that reality is even more complicated. Wearing is allowed up to a certain measure, e.g. 20 mm at Deutsche Bahn (DB). In the present investigation 10 mm were assumed, however uniformly distributed over rail width (cf. Figure 5) as it could be the case after re-profiling. The shift of the contact area towards the rail head centre is, however, the consequence of non-uniform wear such as illustrated in Figure 16. Therefore, the present results are approximate estimates because of which the abscissa in Figure 15 is given qualitatively for relative statements only.

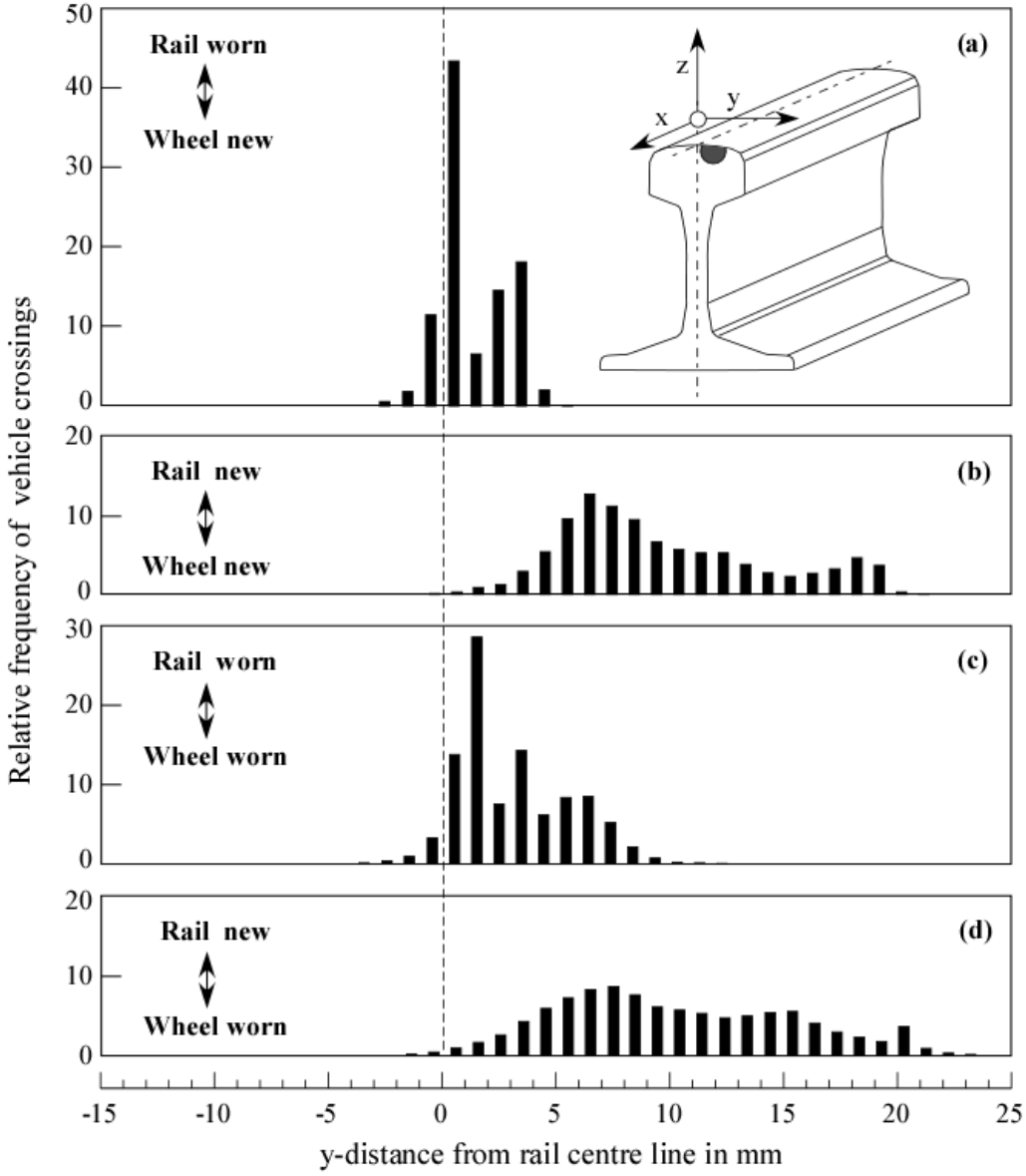

Figure 14: Statistics of roll-over paths of four rail-wheel combinations (Curved track; data according to Deutsche Bahn (DB) Systemtechnik, TZF 63).

Table 1: Probability of occurrence of the four roll-over paths for which K factor solutions have been provided (Appendix) for the rail-wheel combinations of Figure 14.

Roll-over path y	Rail-wheel combination (R = rail; Wh = wheel; N = new; W = worn			
	R/W ↔ Wh/N	R/N ↔ Wh/N	R/W ↔ Wh/W	R/N ↔ Wh/W
-1 mm	65%	2%	47%	3%
4 mm	35%	31%	45%	28%
9 mm	0	46%	8%	41%
17 mm	0	21%	0	28%

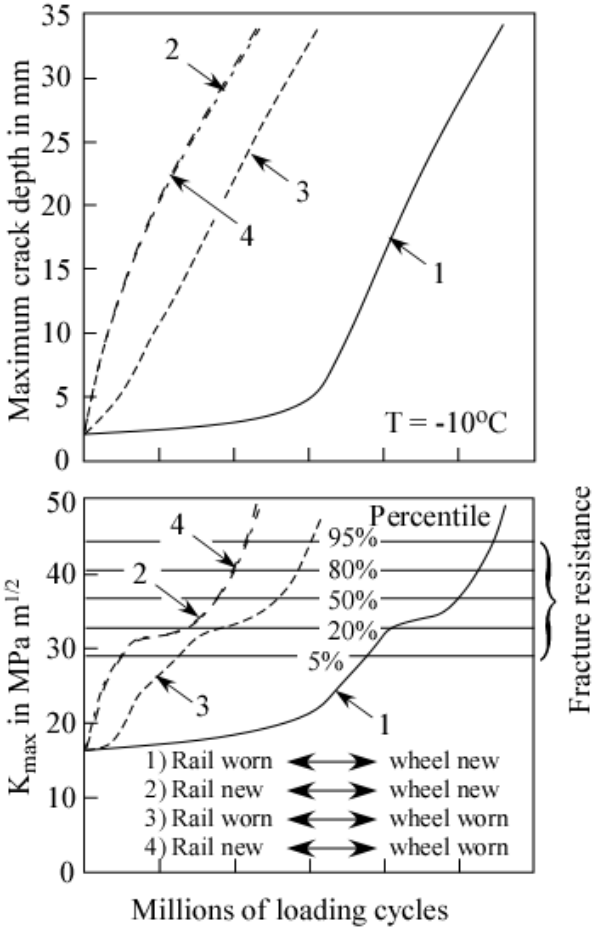

Figure 15: Effect of the rail-wheel combination on fatigue crack extension (top) and the maximum K factor K_{max} (bottom). The fracture toughness percentile values are taken from Figure 13. All calculations have been performed for a constant ambient temperature of -10°C and a semi-circular initial crack of 2 mm depth.

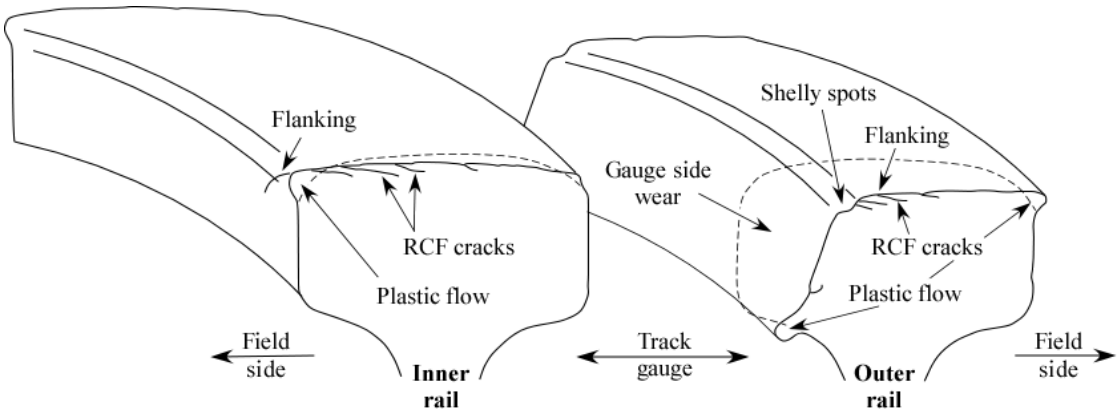

Figure 16: Wear pattern at the outer and inner rail of a curved track (according to [19]).

The different patterns of fatigue crack extension for the four rail-wheel combinations are also illustrated in Figure 17 which shows the development of fatigue crack geometries. As can be seen these tend to a constant value of about a/c = 0.7 after a certain growth. The significant difference in residual lifetime between combinations (1) and (4) is due to the fact that the

crack growth towards the centre or the rail head in case (1) but towards its lower corner in case (4).

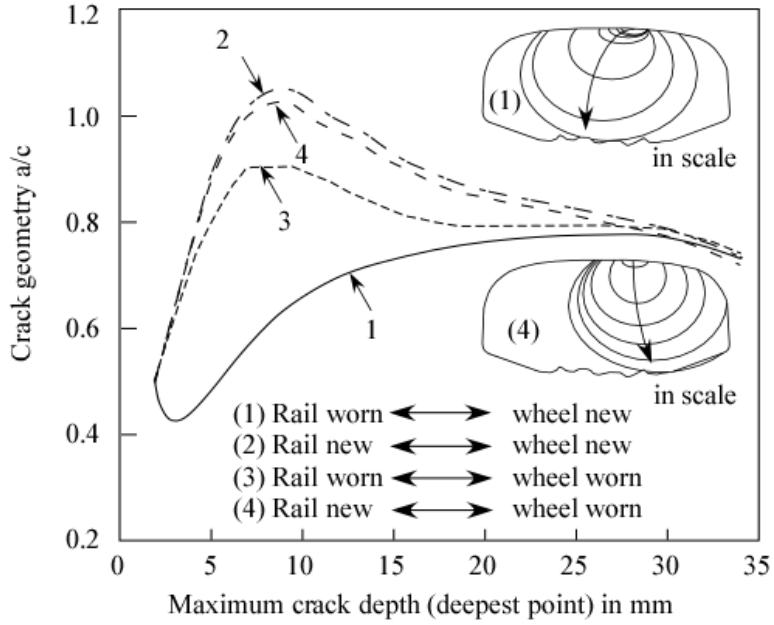

Figure 17: Crack shape development depending on the rail-wheel combination.

3.6 Effects of Seasonal Ambient Temperatures on fatigue crack extension and fracture

The results in Figure 15 were obtained for a constant ambient temperature of -10°C. In reality the ambient temperature changes from day to day as well as during each day. This has to be taken into account for realistic analyses. As mentioned in Section 2 (a) the rail is subjected to tensile thermal stresses at temperatures lower than the rail neutral temperature. What controls the magnitude of these stresses is not the absolute temperature but the temperature difference to the neutral temperature. In addition there is a slight (absolute) temperature effect on fracture toughness as shown in Figure 13. This is, however, of minor importance compared to the temperature dependent variation of the applied K factor.

Note that, with respect to the effect of the ambient temperature, it has to be distinguished between fatigue crack extension and fracture. Whilst the fatigue crack growth is a cumulative process and should therefore be based on average temperatures, e.g. on a daily basis, the fracture event will be controlled by the minimum temperature peaks.

The following examples use ambient temperatures measured 2 metres above the ground at the meteorological station at Kempten (German alpine upland) in 2005 [20]. Two analyses were carried out. For the first one an inspection was assumed in the middle of November, for the second one in the middle of April. It was further assumed that the maximum undetected crack depth was 1 mm in both cases. This was then taken as the depth of a semi-circular initial crack. As rail-wheel combination the case “worn rail-worn wheel” (Figure 14 c; Table 1: R/W ↔ Wh/W) was chosen.

The simulation of fatigue crack extension was based on the average daily temperatures whereas the maximum K factors K_{max} (as the parameters controlling fracture) were determined for the minimum peak temperatures over the same time spans. These are then compared to percentile fracture toughness values for -30°C (Figure 13) in order to

conservatively determine fracture probabilities. The overall time span investigated comprises one year. All results are summarised in Figure 18.

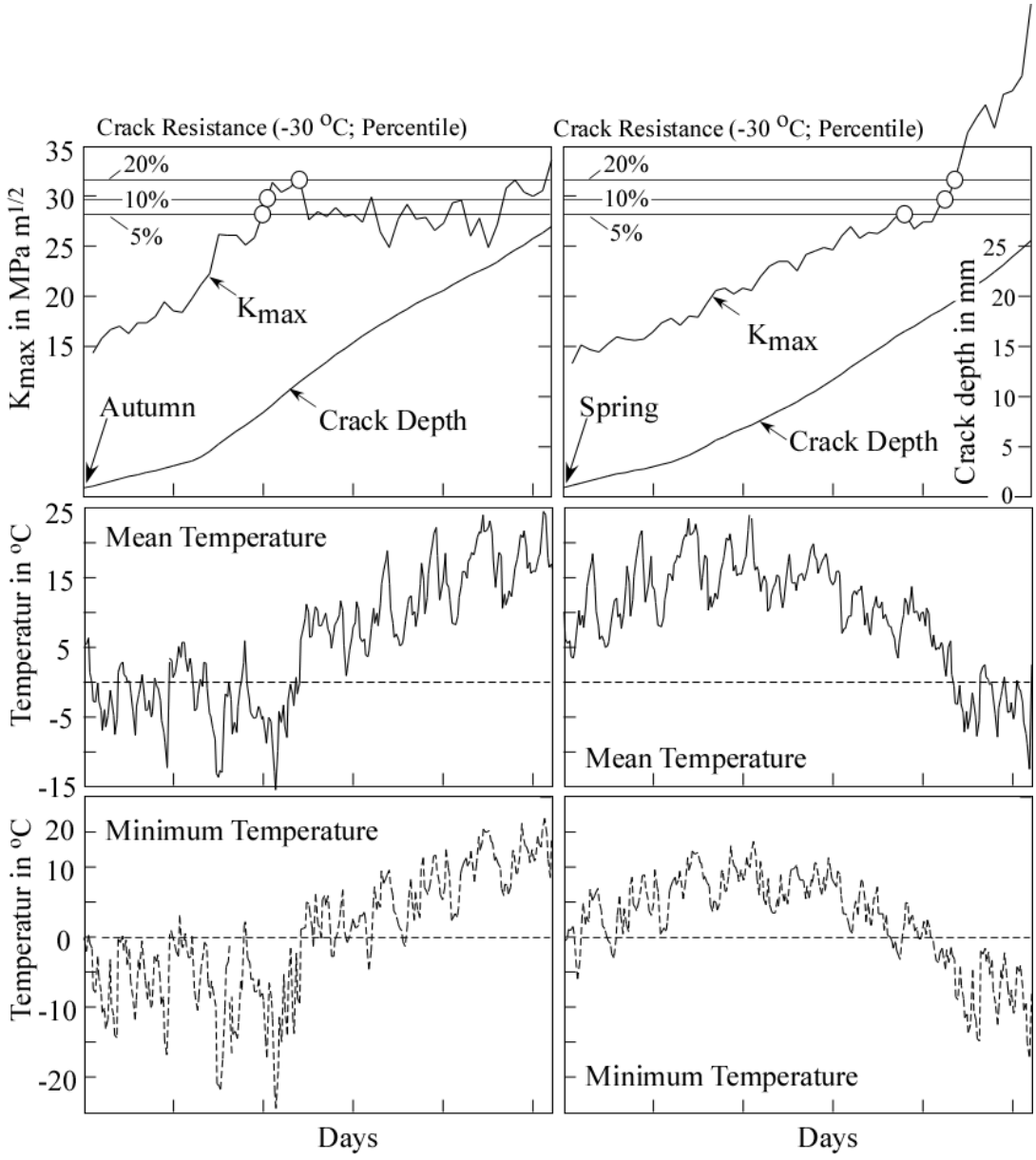

Figure 18: Fatigue crack propagation and maximum K factor K_{max} as functions of calendar date. Left: Last inspection in the middle of November; Right: Last inspection in the middle of April.

Example 1 (Figure 18 left side): An initial crack depth of 1 mm is assumed to exist at the middle of November. The fatigue extension rate of this crack increases significantly at the beginning of the winter time when it becomes colder and decreases, however less pronounced, when it becomes warmer again in spring time. Compared to the crack propagation rate the maximum K factor responds much more sensitively to temperature variations but also to the increasing crack size. At the end of the winter time the failure probability (probability that $K_{max} \geq$ the crack resistance or fracture toughness) reaches a maximum of c. 20%. If the damaged rail survives this time – which will happen with a probability of 80% in the example – the fracture probability decreases reaching a maximum of no more than c. 10% at some colder spring nights until it increases again at late autumn.

Example 2 (Figure 18 right side): This time the existence of a 1 mm deep initial crack is assumed at the middle of April. Crack extension is predicted to accelerate slightly at early autumn and again at early winter time. Whereas it took no more than about 4 months up to a fracture probability greater 10% in Example 1 it takes about twice as long this time because of the higher temperatures from late spring to autumn. However, at the beginning of the winter time the failure probability increases rapidly reaching almost 100% at its end.

The result illustrates what is known from practical experience. Most rail fractures occur during the first cold nights which in Middle Europe usually occur in December or January (Figure 19). Fatigue damaged rails which survive these nights have a good chance also to survive the rest of the winter time.

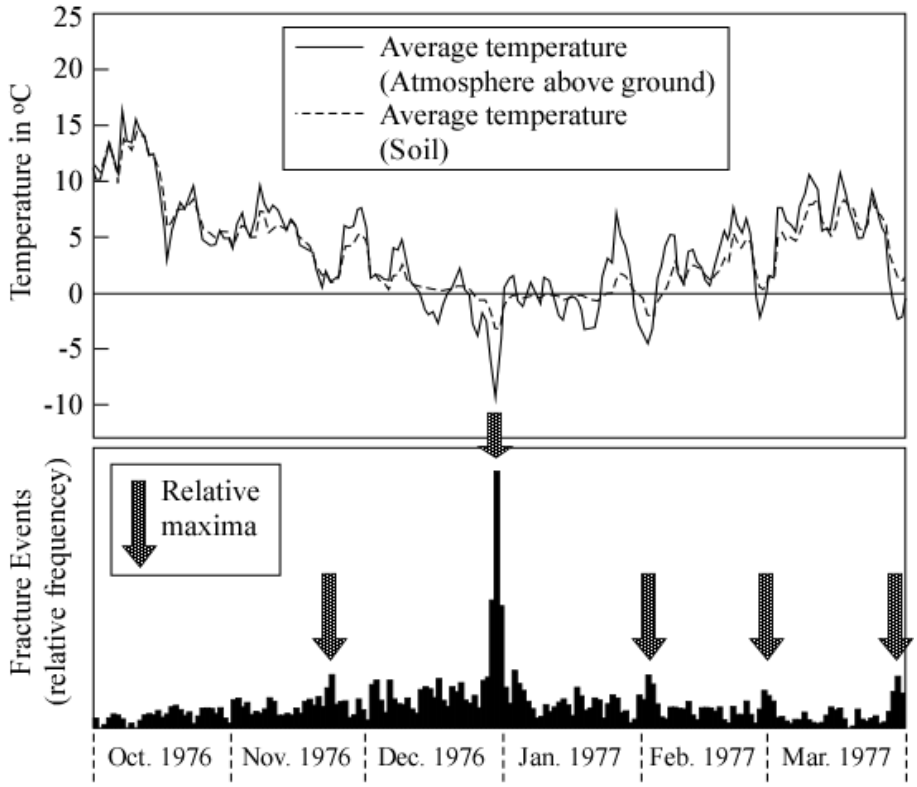

Figure 19: Fracture statistics of rails between autumn 1976 and spring 1977 (former East German rail system, according to [21]).

4. Summary and Conclusions

Methodological investigations on the damage tolerance behaviour of railway rails have been presented which were based on what the authors designated as stage 2 fatigue crack propagation, however, modified for small initial cracks. Due to this and further simplifying assumptions the results should be regarded as first estimates used for identifying trends and the effects of factors such as the local load input and seasonal ambient temperature on fatigue crack propagation and residual lifetime. Nevertheless they were in an order which would allow for a realistic inspection scenario.

In more detail it was found that the fatigue crack propagation rate is affected by the wearing state of the rail as long as the crack is relatively small. Worn rails were of benefit, i.e., they yielded higher residual lifetimes due to the fact that the contact area was shifted to the centre

line of the rail head whereas the initial cracks were assumed to be located away from that position. The initial crack pattern is known from in-service practice and can be explained by the fact that the highest frequency of roll-over paths occurs 5 to 10 mm away from the centre line in new rails in straight or slightly curved tracks. Note, however, that the reduction of the rail head height due to wear reduces the residual lifetime irrespective of fatigue. Despite from the model simplifications it was shown that the varying local load input due to the bogie's side motion is of major importance and should not be ignored in a damage tolerance analysis.

Another effect studied was that of ambient temperature. The larger the difference between the rail neutral temperature from track installation and the operation temperature the higher the thermal stresses built-up in continuously welded rails. At temperatures lower than the neutral temperature these are tensile stresses. In cold wintertime these are highly significant for fatigue crack propagation. The effect of inspections in autumn and spring time on the probable failure time of the rail has been demonstrated by two simulations. As a consequence, in terms of damage tolerance, an inspection in late autumn is much more important than an inspection after the wintertime, at least for the climatic conditions of Middle Europe chosen for the study. Whereas the ambient temperature had a significant but still moderate effect on the fatigue crack extension, it strongly affected the maximum K factor, and as a consequence, the fracture probability of the rail during cold winter nights.

As mentioned the results should be regarded as first estimates. More accurate and more complete investigations should also include mixed transport – in the present paper only high speed trains of the German ICE type were considered. They also should include the effect of different track foundation conditions, ambient temperature sequences at different locations, further wearing states of the rail etc.

3. References

[1] Girardi, L., Heyder, R., Dider, L. and Boulanger, D. (2005): IDR2-NOVUM promises lower rail maintenance costs. Railway Gazette Int. July 2005, 439-441.

[2] Gibson, S. (2005): Incentivising operational performance on the UK rail infrastructure since 1996**.** Utilities Policy 13, 222-229.

[3] Smith, R.A. (1998): Fatigue in transport. Problems, solutions and future threats. Trans. Inst. Chem. E. 76, Part B, 217-223.

[4] Zerbst, U., Smith, R. Lunden, R. and Edel, K.-O. (2008): Damage tolerance of railway rails. Engineering Fracture Mechanics, this issue, xxx-xxx. (Title and order of authors still open).

[5] Cannon, D.F., Edel, K.-O., Grassie, S.L. and Sawley, K. (2003): Rail defects. An overview. Fatigue Fracture Engng. Mat. Struct. 26, 865-886.

[6] Zerbst, U., Mädler, K. and Hintze, H. (2005): Fracture mechanics in railway applications – an overview. Engng. Fracture Mech. 72, 163-194.

[7] Allen R. (2000): Rail defect management: British practice. In: Proceedings of Internationales Symposium Schienenfehler, Brandenburg, Section 14.

[8] Bogdanski, S., Olzak, M und Stupnitzki, J. (1996): Numerical stress analysis of rail rolling contact fatigue cracks. J. Wear 191,14–24.

[9] Bogdanski, S. und Brown, M.W. (2002): Modelling the three-dimensional behaviour of shallow rolling contact fatigue cracks in rails. Wear 253, 17–25.

[10] R. Krull, H. Hintze, M. Thomas, R. Pohl, S. Ruehe (2003): Eddy-current detection of head checks on the gauge corner of rails: recent results. Proceedings 6th International Conference Railway Engineering, London.

[11] Webster, P.J., Wang, X., Mills, G., Kamg, W. and Webster, G.A. (1991): Residual stress measurements on ORE railway rails by neutron diffraction. UIC, Final Report BRSUIC02/91.

[12] Jeong, D.Y. (2003): Correlations between rail defect growth data and engineering analyses. Part I: Laboratory tests. UIC/WEC Joint Research Project on Rail Defect Management, U.S. Dept. of Transportation Res. & Special Programs Administration, Section 3.1: Stress Analyses.

[13] Magiera, J. (2002): Enhanced 3D analysis of residual stress in rails by physically based fit to neutron diffraction data. Wear 253, 228-240.

[14] Richard, H.A. (2003): Festigkeitsnachweis unter Mixed-Mode-Beanspruchung. Materialprüfung 45, S. 513-18.

[15] NASGRO: Fatigue Crack Growth Computor Program „NASGRO“, Version 3. NASA, L.B. Johnson Space Centre, Houston, Texas. JSC-22267B, 2000.

[16] ASTM E 1921-05 (2005): Standard Test Method for Determination of Reference Temperature, T_O, for Ferritic Steels in the Transition Range.

[17] Zerbst, U., Drewett, L. and Schöne, D. (2008): Fatigue and fracture properties of rail steels. Engineering Fracture Mechanics, this issue, xxx-xxx.

[18] Kim, J.J. und Kim C.S. (2002): Fatigue crack growth behavior of rail steel under mode I and mixed mode loadings. Mat. Sci. and Engng. A, 338, 191-201.

[19] Magel, E., Roney, M., Kalousek, J. and Sroba, P. (2003): The blending of theory and practice in modern rail grinding. Fatigue Fracture Engng. Mat. Struct. 26, 921-929.

[20] Deutscher Wetterdienst (DWD): http://www.dwd.de/de/FundE/Klima/ KLIS/daten/online/nat/index_tageswerte.htm

[21] Edel, K.-O. (1979): Temperaturabhängigkeit des Auftretens von Schienenbrüchen. Signal und Schiene 6/1979, 266-272.

Acknowledgment: The authors wish to thank Dr. B. Ripke, Deutsche Bahn (DB) Systemtechnik, TZF 62, for providing the loading data and V. Sauer, DB Systemtechnik, TZF 63, for providing the roll-over statistics. The residual stress data were made available by Y. Bourdon of Corus Rail, Hayange.

Appendix: K Factor Solutions

Table A1: K factor solutions for thermal stress loading:
$K_I^T = Y_I^T \cdot (\Delta T/\Delta T_0)$; $K_{II}^T = Y_{II}^T \cdot (\Delta T/\Delta T_0)$; $K_{III}^T = Y_{III}^T \cdot (\Delta T/\Delta T_0)$;
K_I^T, K_{II}^T and K_{III}^T in MPa $mm^{1/2}$; $\Delta T_0 = 100\ ^0C$.

a in mm	a/c	Point A			Point B			Point C		
		$Y_I^T(A)$	$Y_{II}^T(A)$	$Y_{III}^T(A)$	$Y_I^T(B)$	$Y_{II}^T(B)$	$Y_{III}^T(B)$	$Y_I^T(C)$	$Y_{II}^T(C)$	$Y_{III}^T(C)$
2	0.25	482	-122	0	310	-25	100	290	-50	-40
	0.50	438	-115	0	320	0	120	310	-20	-80
	0.75	382	-110	0	330	20	100	325	0	-90
5	0.45	818	-220	0	637	58	160	702	50	-175
	0.65	701	-212	0	645	35	166	676	32	-168
	0.85	603	-203	0	632	41	167	662	51	-168
10	0.60	1170	-344	0	1000	61	273	1114	80	-290
	0.75	1020	-330	0	999	77	270	1060	85	-275
	0.95	870	-312	0	952	52	270	970	43	-261
15	0.65	1525	-449	0	1404	78	345	1670	80	-393
	0.80	1278	-427	0	1315	60	335	1439	75	-350
	1.00	1068	-395	0	1227	49	325	1270	47	-330
20	0.70	2075	-560	0	1900	56	430	2755	28	-600
	0.85	1585	-511	0	1683	45	400	1949	38	-457
	1.00	1335	-471	0	1550	38	390	1667	21	-411

Table A2: K factor solutions for residual stress loading:
$K_I^R = Y_I^R$; $K_{II}^R = Y_{II}^R$; $K_{III}^R = Y_{III}^R$; K_I^R, K_{II}^R and K_{III}^R in MPa $mm^{1/2}$.

a in mm	a/c	Point A			Point B			Point C		
		$Y_I^R(A)$	$Y_{II}^R(A)$	$Y_{III}^R(A)$	$Y_I^R(B)$	$Y_{II}^R(B)$	$Y_{III}^R(B)$	$Y_I^R(C)$	$Y_{II}^R(C)$	$Y_{III}^R(C)$
2	0.25	390	-91	2	250	-20	90	200	-50	-50
	0.50	350	-86	2	260	0	100	250	-25	-80
	0.75	307	-83	1	270	10	90	270	-15	-80
5	0.45	550	-115	3	500	46	120	525	29	-125
	0.65	458	-112	3	500	28	126	515	21	-125
	0.85	386	-107	2	497	34	128	513	35	-127
10	0.60	415	-81	7	610	29	155	650	28	-155
	0.75	332	-77	5	620	40	154	640	36	-152
	0.95	257	-70	3	582	27	148	590	16	-146
15	0.65	307	-37	9	560	22	120	630	15	-127
	0.80	210	-33	7	523	16	115	552	13	-115
	1.00	137	-26	4	485	13	111	489	5	-109
20	0.70	190	24	2	500	5	95	690	-9	-127
	0.85	70	28	3	445	3	85	490	-5	-100
	1.00	15	30	2	415	2	80	410	-8	-83

Table A3: K factor solutions for axle loading (Roll-over path 1: y = -1 mm; max. load in loading cycle); $K_I^{L1} = Y_I^{L1} \cdot (F/F_0)$; $K_{II}^{L1} = Y_{II}^{L1} \cdot (F/F_0)$; $K_{III}^{L1} = Y_{III}^{L1} \cdot (F/F_0)$; K_I^{L1}, K_{II}^{L1} and K_{III}^{L1} in MPa mm$^{1/2}$; F_0 = 107.9 kN.

a in mm	a/c	Point A			Point B			Point C		
		Y_I^{L1}(A)	Y_{II}^{L1}(A)	Y_{III}^{L1}(A)	Y_I^{L1}(B)	Y_{II}^{L1}(B)	Y_{III}^{L1}(B)	Y_I^{L1}(C)	Y_{II}^{L1}(C)	Y_{III}^{L1}(C)
2	0.25	12	60	0	7	0	0	7	0	26
	0.50	11	58	0	7	0	0	7	0	55
	0.75	10	56	0	7	0	0	7	0	60
5	0.45	19	190	0	16	0	0	17	0	76
	0.65	16	171	0	16	0	0	17	0	75
	0.85	14	156	0	16	0	0	17	0	78
10	0.60	25	259	0	22	0	0	25	0	117
	0.75	21	236	0	22	0	0	24	0	120
	0.95	18	215	0	21	0	0	22	0	127
15	0.65	30	238	0	30	0	0	35	0	153
	0.80	25	216	0	28	0	0	30	0	151
	1.00	20	189	0	26	0	0	27	0	157
20	0.70	38	222	0	38	0	0	56	0	217
	0.85	29	192	0	33	0	0	39	0	182
	1.00	24	169	0	31	0	0	34	0	175

Table A4: K factor solutions for axle loading (Roll-over path 1: y = -1 mm; min. load in loading cycle); $K_I^{L1} = Y_I^{L1} \cdot (F/F_0)$; $K_{II}^{L1} = Y_{II}^{L1} \cdot (F/F_0)$; $K_{III}^{L1} = Y_{III}^{L1} \cdot (F/F_0)$; K_I^{L1}, K_{II}^{L1} and K_{III}^{L1} in MPa mm$^{1/2}$; F_0 = 107.9 kN.

a in mm	a/c	Point A			Point B			Point C		
		Y_I^{L1}(A)	Y_{II}^{L1}(A)	Y_{III}^{L1}(A)	Y_I^{L1}(B)	Y_{II}^{L1}(B)	Y_{III}^{L1}(B)	Y_I^{L1}(C)	Y_{II}^{L1}(C)	Y_{III}^{L1}(C)
2	0.25	-267	55	0	-800	-150	-40	0	25	0
	0.50	-234	55	0	-350	-100	-25	-100	25	0
	0.75	-200	53	0	-280	-90	-30	-180	25	0
5	0.45	-586	-140	0	-1150	-65	-350	-360	-20	0
	0.65	-466	-108	0	-1065	106	-325	-375	-28	0
	0.85	-399	-90	0	-1035	185	-270	-385	-30	0
10	0.60	-650	-330	0	-810	-225	-215	-515	-95	0
	0.75	-541	-300	0	-1035	-198	-295	-515	-115	0
	0.95	-432	-250	0	-1070	-85	-345	-495	-125	0
15	0.65	-580	-275	0	-710	-155	-180	-685	-105	0
	0.80	-472	-218	0	-765	-140	-215	-620	-96	0
	1.00	-379	-155	0	-840	-85	-253	-577	-82	0
20	0.70	-586	-162	0	-735	-50	-185	-950	-63	0
	0.85	-440	-158	0	-705	-55	-200	-705	-55	0
	1.00	-360	-146	0	-695	-53	-215	-620	-54	0

Table A5: K factor solutions for axle loading (Roll-over path 2: y = 4 mm; max. load in loading cycle); $K_I^{L2} = Y_I^{L2} \cdot (F/F_0)$; $K_{II}^{L2} = Y_{II}^{L2} \cdot (F/F_0)$; $K_{III}^{L2} = Y_{III}^{L2} \cdot (F/F_0)$; K_I^{L2}, K_{II}^{L2} and K_{III}^{L2} in MPa mm$^{1/2}$; F_0 = 107.9 kN.

a in mm	a/c	Point A			Point B			Point C		
		Y_I^{L2}(A)	Y_{II}^{L2}(A)	Y_{III}^{L2}(A)	Y_I^{L2}(B)	Y_{II}^{L2}(B)	Y_{III}^{L2}(B)	Y_I^{L2}(C)	Y_{II}^{L2}(C)	Y_{III}^{L2}(C)
2	0.25	12	74	0	7	0	0	7	0	35
	0.50	11	73	0	7	0	0	7	0	68
	0.75	10	71	0	7	0	0	7	0	70
5	0.45	19	286	0	16	0	0	17	0	82
	0.65	16	245	0	16	0	0	17	0	83
	0.85	14	247	0	16	0	0	17	0	91
10	0.60	25	295	0	22	0	0	25	0	127
	0.75	21	237	0	22	0	0	24	0	121
	0.95	18	246	0	21	0	0	22	0	150
15	0.65	30	250	0	30	0	0	35	0	167
	0.80	25	230	0	28	0	0	30	0	170
	1.00	20	203	0	26	0	0	27	0	180
20	0.70	38	229	0	38	0	0	56	0	235
	0.85	29	200	0	33	0	0	39	0	200
	1.00	24	177	0	31	0	0	34	0	195

Table A6: K factor solutions for axle loading (Roll-over path 2: y = 4 mm; min. load in loading cycle); $K_I^{L2} = Y_I^{L2} \cdot (F/F_0)$; $K_{II}^{L2} = Y_{II}^{L2} \cdot (F/F_0)$; $K_{III}^{L2} = Y_{III}^{L2} \cdot (F/F_0)$; K_I^{L2}, K_{II}^{L2} and K_{III}^{L2} in MPa mm$^{1/2}$; F_0 = 107.9 kN.

a in mm	a/c	Point A			Point B			Point C		
		Y_I^{L2}(A)	Y_{II}^{L2}(A)	Y_{III}^{L2}(A)	Y_I^{L2}(B)	Y_{II}^{L2}(B)	Y_{III}^{L2}(B)	Y_I^{L2}(C)	Y_{II}^{L2}(C)	Y_{III}^{L2}(C)
2	0.25	-325	47	0	-1000	-300	-80	-200	30	0
	0.50	-280	46	0	-1400	-200	-15	-200	60	0
	0.75	-243	50	0	-500	-150	-15	-200	55	0
5	0.45	-803	-327	0	-1100	-200	-170	-420	-27	0
	0.65	-720	-364	0	-1500	-100	-255	-470	-50	0
	0.85	-570	-255	0	-1550	0	-425	-500	-50	0
10	0.60	-735	-438	0	-690	-192	-165	-570	-105	0
	0.75	-541	-300	0	-1100	-200	-292	-520	-112	0
	0.95	-516	-370	0	-1030	-245	-285	-595	-158	0
15	0.65	-610	-328	0	-670	-144	-160	-735	-117	0
	0.80	-497	-253	0	-710	-135	-187	-690	-110	0
	1.00	-397	-173	0	-765	-92	-223	-660	-89	0
20	0.70	-600	-175	0	-715	-45	-170	-1000	-70	0
	0.85	-452	-170	0	-680	-52	-182	-750	-60	0
	1.00	-370	-160	0	-660	-55	-196	-670	-59	0

Table A7: K factor solutions for axle loading (Roll-over path 3: y = 9 mm; max. load in loading cycle); $K_I^{L3} = Y_I^{L3} \cdot (F/F_0)$; $K_{II}^{L3} = Y_{II}^{L3} \cdot (F/F_0)$; $K_{III}^{L3} = Y_{III}^{L3} \cdot (F/F_0)$; K_I^{L3}, K_{II}^{L3} and K_{III}^{L3} in MPa mm$^{1/2}$; F_0 = 107.9 kN.

a in mm	a/c	Point A			Point B			Point C		
		Y_I^{L3}(A)	Y_{II}^{L3}(A)	Y_{III}^{L3}(A)	Y_I^{L3}(B)	Y_{II}^{L3}(B)	Y_{III}^{L3}(B)	Y_I^{L3}(C)	Y_{II}^{L3}(C)	Y_{III}^{L3}(C)
2	0.25	12	420	0	7	0	0	7	0	60
	0.50	11	410	0	7	0	0	7	0	110
	0.75	10	395	0	7	0	0	7	0	120
5	0.45	19	436	0	16	0	0	17	0	95
	0.65	16	400	0	16	0	0	17	0	125
	0.85	14	395	0	16	0	0	17	0	185
10	0.60	25	316	0	22	0	0	25	0	160
	0.75	21	296	0	22	0	0	24	0	195
	0.95	18	270	0	21	0	0	22	0	235
15	0.65	30	253	0	30	0	0	35	0	200
	0.80	25	230	0	28	0	0	30	0	212
	1.00	20	205	0	26	0	0	27	0	238
20	0.70	38	230	0	38	0	0	56	0	275
	0.85	29	197	0	33	0	0	39	0	238
	1.00	24	170	0	31	0	0	34	0	233

Table A8: K factor solutions for axle loading (Roll-over path 3: y = 9 mm; min. load in loading cycle); $K_I^{L3} = Y_I^{L3} \cdot (F/F_0)$; $K_{II}^{L3} = Y_{II}^{L3} \cdot (F/F_0)$; $K_{III}^{L3} = Y_{III}^{L3} \cdot (F/F_0)$; K_I^{L3}, K_{II}^{L3} and K_{III}^{L3} in MPa mm$^{1/2}$; F_0 = 107.9 kN.

a in mm	a/c	Point A			Point B			Point C		
		Y_I^{L3}(A)	Y_{II}^{L3}(A)	Y_{III}^{L3}(A)	Y_I^{L3}(B)	Y_{II}^{L3}(B)	Y_{III}^{L3}(B)	Y_I^{L3}(C)	Y_{II}^{L3}(C)	Y_{III}^{L3}(C)
2	0.25	-1238	-550	0	-500	70	-100	-300	70	0
	0.50	-1200	-570	0	-1200	100	-150	-400	100	0
	0.75	-1090	-577	0	-900	70	-240	-1100	50	0
5	0.45	-1163	-650	0	-530	-55	-84	-580	-22	0
	0.65	-1040	-635	0	-775	-127	-130	-780	-86	0
	0.85	-940	-655	0	-1040	-170	-200	-1025	-110	0
10	0.60	-772	-485	0	-547	-130	-121	-690	-130	0
	0.75	-670	-465	0	-620	-170	-150	-770	-165	0
	0.95	-565	-427	0	-680	-210	-182	-840	-210	0
15	0.65	-625	-325	0	-590	-110	-133	-830	-130	0
	0.80	-505	-267	0	-600	-115	-147	-800	-130	0
	1.00	-405	-185	0	-615	-90	-167	-810	-96	0
20	0.70	-615	-190	0	-665	-36	-148	-1070	-86	0
	0.85	-465	-185	0	-615	-50	-154	-820	-70	0
	1.00	-380	-170	0	-590	-55	-162	-750	-65	0

Table A9: K factor solutions for axle loading (Roll-over path 4: y = 17 mm; max. load in loading cycle); $K_I^{L4} = Y_I^{L4} \cdot (F/F_0)$; $K_{II}^{L4} = Y_{II}^{L4} \cdot (F/F_0)$; $K_{III}^{L4} = Y_{III}^{L4} \cdot (F/F_0)$; K_I^{L4}, K_{II}^{L4} and K_{III}^{L4} in MPa mm$^{1/2}$; F_0 = 107.9 kN.

a in mm	a/c	Point A			Point B			Point C		
		Y_I^{L4}(A)	Y_{II}^{L4}(A)	Y_{III}^{L4}(A)	Y_I^{L4}(B)	Y_{II}^{L4}(B)	Y_{III}^{L4}(B)	Y_I^{L4}(C)	Y_{II}^{L4}(C)	Y_{III}^{L4}(C)
2	0.25	12	113	0	7	0	0	7	0	30
	0.50	11	105	0	7	0	0	7	0	110
	0.75	10	100	0	7	0	0	7	0	45
5	0.45	19	243	0	16	0	0	17	0	275
	0.65	16	220	0	16	0	0	17	0	410
	0.85	14	197	0	16	0	0	17	0	265
10	0.60	25	247	0	22	0	0	25	0	245
	0.75	21	226	0	22	0	0	24	0	317
	0.95	18	199	0	21	0	0	22	0	327
15	0.65	30	218	0	30	0	0	35	0	262
	0.80	25	195	0	28	0	0	30	0	285
	1.00	20	167	0	26	0	0	27	0	293
20	0.70	38	214	0	38	0	0	56	0	338
	0.85	29	178	0	33	0	0	39	0	290
	1.00	24	152	0	31	0	0	34	0	275

Table A10: K factor solutions for axle loading (Roll-over path 4: y = 17 mm; min. load in loading cycle); $K_I^{L4} = Y_I^{L4} \cdot (F/F_0)$; $K_{II}^{L4} = Y_{II}^{L4} \cdot (F/F_0)$; $K_{III}^{L4} = Y_{III}^{L4} \cdot (F/F_0)$; K_I^{L4}, K_{II}^{L4} and K_{III}^{L4} in MPa mm$^{1/2}$; F_0 = 107.9 kN.

a in mm	a/c	Point A			Point B			Point C		
		Y_I^{L4}(A)	Y_{II}^{L4}(A)	Y_{III}^{L4}(A)	Y_I^{L4}(B)	Y_{II}^{L4}(B)	Y_{III}^{L4}(B)	Y_I^{L4}(C)	Y_{II}^{L4}(C)	Y_{III}^{L4}(C)
2	0.25	-435	30	0	-150	40	-70	-400	-100	0
	0.50	-368	33	0	-190	40	-100	-850	-50	0
	0.75	-315	35	0	-220	40	-80	-1100	50	0
5	0.45	-720	-187	0	-347	-27	-65	-1125	-45	0
	0.65	-575	-150	0	-390	-33	-78	-1110	0	0
	0.85	-487	-150	0	-405	-45	-87	-1175	165	0
10	0.60	-627	-235	0	-440	-75	-95	-985	-140	0
	0.75	-520	-220	0	-465	-100	-103	-1140	-42	0
	0.95	-415	-185	0	-455	-110	-115	-1025	68	0
15	0.65	-570	-200	0	-515	-75	-110	-968	-120	0
	0.80	-465	-190	0	-500	-75	-115	-985	-101	0
	1.00	-370	-135	0	-475	-60	-122	-940	-41	0
20	0.70	-620	-173	0	-595	-15	-123	-1185	-92	0
	0.85	-466	-165	0	-540	-26	-125	-927	-60	0
	1.00	-380	-152	0	-503	-32	-127	-845	-41	0

Symbols

a	crack depth dimension (Figure 7)
2c	crack length dimension (Figure 7)
da/dN	fatigue crack propagation rate
K	stress intensity factor, K factor
K_I	K factor for mode I crack opening
K_{II}	K factor for mode II crack opening
K_{III}	K factor for mode III crack opening
K_c	Fracture resistance of the material
K_{max}	maximum K value of a loading cycle
K_{min}	miximum K value of a loading cycle
K_v	equivalent K factor for mixed mode loading
N	number of loading cycles
R	cyclic loading ratio = K_{min}/K_{max}
T	temperature
ΔK	cyclic K factor = K_{max} - K_{min}
ΔK_I	cyclic K factor for mode I crack opening
ΔK_{II}	cyclic K factor for mode II crack opening
ΔK_{III}	cyclic K factor for mode III crack opening
ΔK_v	equivalent cyclic K factor for mixed mode loading
σ	stress, general
σ_x	axial component of residual stresses due to roller straightening (Figure 8)